BIOMOLECULES & THERAPEUTICS

Original Article
Biomol Ther 27(4), 395-403 (2019)

Purpurogallin Protects Keratinocytes from Damage and Apoptosis Induced by Ultraviolet B Radiation and Particulate Matter 2.5

Ao Xuan Zhen[1], Mei Jing Piao[1], Yu Jae Hyun[1], Kyoung Ah Kang[1], Yea Seong Ryu[1], Suk Ju Cho[1], Hee Kyoung Kang[1], Young Sang Koh[1], Mee Jung Ahn[2], Tae Hoon Kim[3] and Jin Won Hyun[1,*]

[1]Jeju National University School of Medicine and Jeju Research Center for Natural Medicine, Jeju 63243,
[2]Laboratory of Veterinary Anatomy, College of Veterinary Medicine, Jeju National University, Jeju 63243,
[3]Department of Food Science and Biotechnology, Daegu University, Gyeongsan 38453, Republic of Korea

Abstract

Purpurogallin, a natural phenol obtained from oak nutgalls, has been shown to possess antioxidant, anticancer, and anti-inflammatory effects. Recently, in addition to ultraviolet B (UVB) radiation that induces cell apoptosis via oxidative stress, particulate matter 2.5 ($PM_{2.5}$) was shown to trigger excessive production of reactive oxygen species. In this study, we observed that UVB radiation and $PM_{2.5}$ severely damaged human HaCaT keratinocytes, disrupting cellular DNA, lipids, and proteins and causing mitochondrial depolarization. Purpurogallin protected HaCaT cells from apoptosis induced by UVB radiation and/or $PM_{2.5}$. Furthermore, purpurogallin effectively modulates the pro-apoptotic and anti-apoptotic proteins under UVB irradiation via caspase signaling pathways. Additionally, purpurogallin reduced apoptosis via MAPK signaling pathways, as demonstrated using MAPK-p38, ERK, and JNK inhibitors. These results indicate that purpurogallin possesses antioxidant effects and protects cells from damage and apoptosis induced by UVB radiation and $PM_{2.5}$.

Key Words: Purpurogallin, Ultraviolet B radiation, Particulate matter 2.5, Oxidative stress, Human HaCaT keratinocytes

INTRODUCTION

Solar radiation is necessary for the synthesis of vitamin D in humans; however, ultraviolet (UV) radiation has been implicated in numerous skin disorders, including tumorigenesis (Feehan *et al*., 2016). UVB irradiation has been shown to cause inflammation and skin cancer (Glady *et al*., 2018; Hosseini *et al*., 2018) through cellular DNA damage or immunosuppression (Nohynek and Schaefer, 2001). An abnormal increase in intracellular reactive oxygen species (ROS), including the hydroxyl radical, induces destruction of cytoskeleton and apoptosis (Kong *et al*., 2016; Zheng *et al*., 2018). Furthermore, excessive ROS levels strain the antioxidant defense systems, resulting in oxidative stress and skin damage (Zheng *et al*., 2014).

Recently, alongside UVB, particulate matter 2.5 ($PM_{2.5}$) has become the focus of public health research, including research on skin hazards. $PM_{2.5}$ represents outdoor air pollution and mainly consists of metals, allergens, toxic products of combustion of fossil fuels and endotoxins (He *et al*., 2016). PM was shown to damage the nervous system (Wang *et al*., 2017), respiratory epithelium (Liu *et al*., 2017), immune system (Castañeda *et al*., 2018) and cardiovascular system (Cao *et al*., 2016). As skin and keratinocytes form the outermost barrier directly facing harmful PM, the combined effects of UVB and $PM_{2.5}$ on the skin are worth investigating.

Phenolic compounds were shown to possess antioxidant effects in cardiovascular diseases, anticancer activity, antiplatelet aggregation effects and anti-bacterial activity (Faggio *et al*., 2017). Furthermore, high levels of polyphenols promote collagen synthesis and protect human skin from photo-aging (Kang *et al*., 2018). Purpurogallin (PG), a natural phenol, suppressed delayed vasospasm, and protected cardiac and kidney cells (Zeng *et al*., 1992; Wu *et al*., 1996; Chang *et al*., 2014). Additionally, PG reduced inflammation in BV2 microglia cells and osteolytic diseases and showed antioxidant effects by scavenging hydroxyl radicals (Prasad and Laxdal, 1994; Park *et al*., 2013; Kim *et al*., 2018).

UVB and $PM_{2.5}$ aggravate the damage to keratinocytes and PG may possess cytoprotective effects. Hence, in this study,

Open Access **https://doi.org/10.4062/biomolther.2018.151**

Received Aug 7, 2018 **Revised** Sep 13, 2018 **Accepted** Oct 6, 2018
Published Online Nov 12, 2018

***Corresponding Author**
E-mail: jinwonh@jejunu.ac.kr
Tel: +82-64-754-3838, Fax: +82-64-702-2687

we explored the antioxidant and cytoprotective effects of PG against UVB- and/or $PM_{2.5}$-induced oxidative stress in HaCaT cells and investigated the underlying mechanisms.

MATERIALS AND METHODS

Reagents and chemicals

Purpurogallin (PG), Diesel particulate matter NIST SRM 1650b ($PM_{2.5}$), 3-(4,5-dimethylthiazol-2-yl)-2,5-diphenyltetrazolium bromide (MTT), 1,1-diphenyl-2-picrylhydrazyl (DPPH), 2′,7′-dichlorofluorescein diacetate (DCF-DA), Primary antibodies anti-caspase-3, anti-caspase-9, 5,5-dimethyl-1-pyrroline-N-oxide (DMPO), Hoechst 33342, caspase inhibitor (Z-VAD-FMK), and p38 MAPK inhibitor (SB203580) were obtained from Sigma-Aldrich (St. Louis, MO, USA). Diphenyl-1-pyrenylphosphine (DPPP) was purchased from Molecular Probes (Eugene, OR, USA). 5,5′,6,6′-tetrachloro-1,1′,3,3′-tetraethylbenzimidazolylcarbocyanine iodide (JC-1) was provided by Invitrogen (Carlsbad, CA, USA). SP600125 and U0126 were purchased from Tocris (Bristol, UK) and Calbiochem (La Jolla, CA, USA), respectively. Primary antibodies anti-Bax, anti-Bcl-2, anti-p38, and anti-PARP were purchased from Santa Cruz Biotechnology Inc (Dallas, TX, USA). Primary antibodies anti-ERK and anti-JNK were purchased from Cell Signaling Technology (Beverly, MA, USA). Anti-IgG secondary antibodies were purchased from Pierce (Rockford, IL, USA). All other chemicals and reagents were of analytical grade.

Cell culture and UVB radiation

Human HaCaT keratinocytes were provided by the AmorePacific Corporation (Yongin, Korea). Cells were maintained in Dulbecco's modified Eagle medium (10% fetal bovine serum, 100 units/ml penicillin, 100 μg/ml streptomycin, and 0.25 μg/ml amphotericin B) at 37°C in humidified atmosphere containing 5% CO_2 (Life Technologies Co., Grand Island, NY, USA). The UVB energy spectrum (280-320 nm) was supplied by CL-1000M UV Crosslinker (UVP, Upland, CA, USA). UVB irradiation dose was 30 mJ/cm^2.

Cell viability

MTT assay was used to assess the cytotoxicity of PG and UVB. Cells (1.0×10^5 cells/well) were plated into a 24-well plate. After 16 h incubation, the cells were exposed to 2.5, 5, or 10 μM PG or UVB radiation. MTT stock solution (2 mg/ml) was added and the cells were incubated for 4 h to yield formazan crystals, which were dissolved in dimethyl sulfoxide (DMSO). Finally, the absorbance was detected at 540 nm using a scanning multi-well spectrophotometer.

DPPH radical detection

PG (2.5, 5, or 10 μM) was mixed with 0.1 mM DPPH, shaken gently, and kept in the dark for 3 h. Residual DPPH was determined at 520 nm using a spectrophotometer.

Determination of intracellular ROS

The ability of PG to inhibit production of intracellular ROS induced by H_2O_2 (1 mM) or UVB radiation (30 mJ/cm^2) was examined using DCF-DA. Cells (1×10^5 cells/well) were seeded in a 96-well plate. After 16 h incubation, 2.5, 5, or 10 μM PG was added, the cells were incubated for 1 h, and treated with H_2O_2 or exposed to UVB radiation. DCF-DA (25 μM) was added to each well and cells were incubated for 10 min. Finally, the fluorescence of 2′,7′-dichlorofluorescein was assessed using a LS-5B spectrofluorometer (Perkin-Elmer, Waltham, MA, USA).

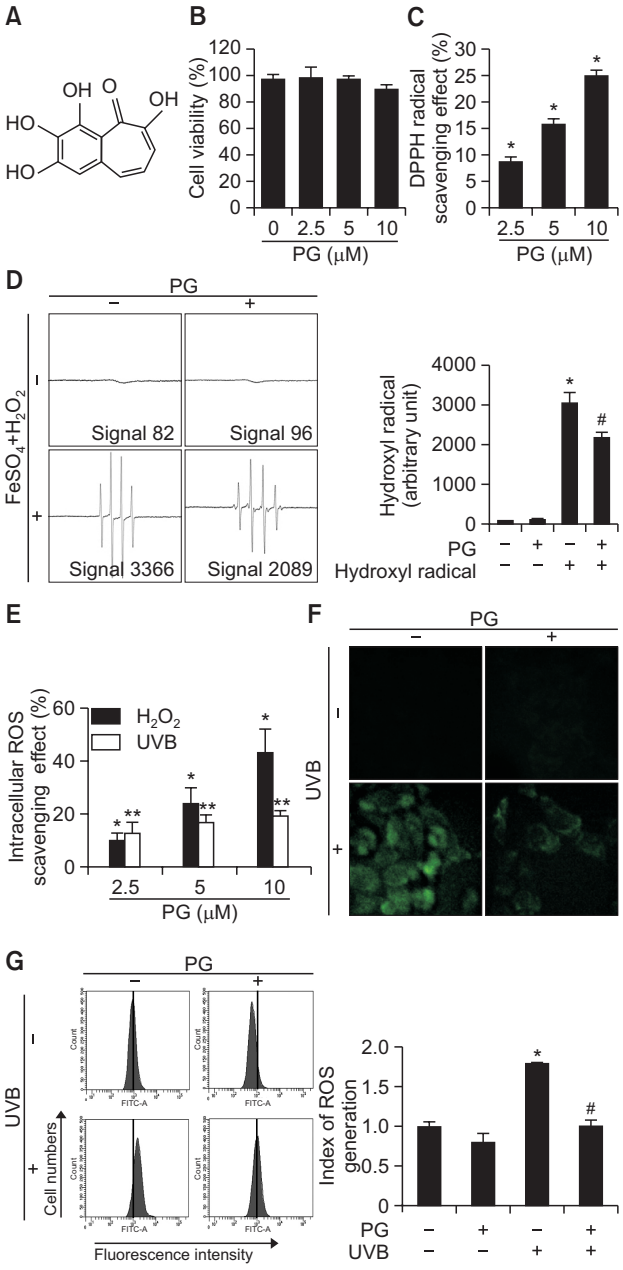

Fig. 1. PG reduced ROS generation. (A) Chemical structure of purpurogallin. (B) The MTT assay was used to determine cell viability after treating HaCaT cells with PG (0, 2.5, 5, 10 μM) for 24 h. (C) DPPH radical scavenging activity of PG (0, 2.5, 5, 10 μM). (D) Hydroxyl radical scavenging potential of PG (10 μM) was estimated using the Fenton reaction. *p<0.05 vs. control cells, $^{\#}p$<0.05 vs. hydroxyl radical. (E) Intracellular ROS scavenging potential of PG (2.5, 5, 10 μM). ROS generated by H_2O_2 or UVB were detected using the DCF-DA assay. *p<0.05 vs. H_2O_2-treated cells, **p<0.05 vs. UVB-irradiated cells. (F) Confocal microscopy and (G) flow cytometry were used for detecting intracellular ROS after DCF-DA staining. *p<0.05 vs. control cells, $^{\#}p$<0.05 vs. UVB-irradiated cells.

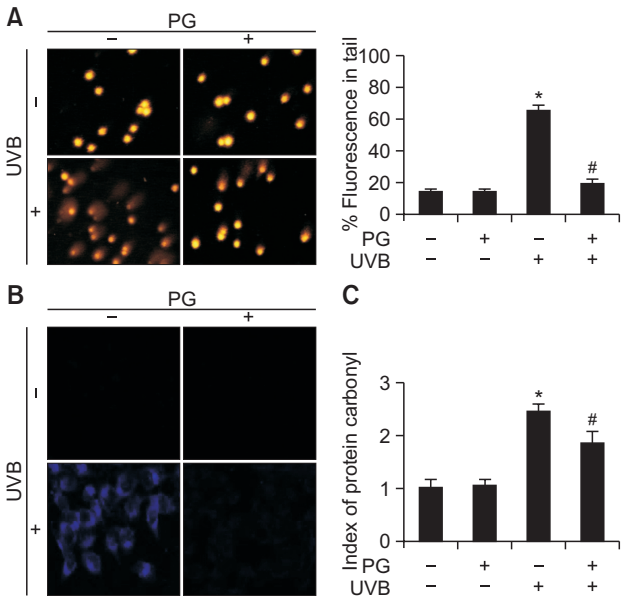

Fig. 2. PG protected cells from UVB-induced damage to macromolecules. (A) The comet assay was used to detect DNA damage. (B) Confocal microscopy was used for detecting lipid peroxidation after DPPP (blue) staining. (C) Protein carbonylation was determined using a protein carbonyl ELISA kit. *p<0.05 vs. control, $^{\#}p$<0.05 vs. UVB-irradiated cells.

Additionally, cells (1.5×10^5 cells/well) were seeded for 16 h, treated with 10 μM PG, and exposed to UVB (30 mJ/cm^2) and/or $PM_{2.5}$ (50 μg/ml) at 37°C. Data were collected after staining the cells with DCF-DA (25 μM) for 30 min at 37°C. Imaging analysis of intracellular ROS was conducted using a confocal microscope (Carl Zeiss, Oberkochen, Germany), whereas stained cells were counted using a flow cytometer (Becton Dickinson, Mountain View, CA, USA).

Hydroxyl radical scavenging

Hydroxyl radical scavenging was assessed after the reaction of DMPO with hydroxyl radicals generated in the Fenton reaction ($FeSO_4$+H_2O_2). An electron spin resonance (ESR) spectrometer was used to detect the resultant DMPO/·OH adduct (Oh *et al.*, 2016). Briefly, 0.3 M DMPO, 10 mM $FeSO_4$, 10 mM H_2O_2, and 10 μM PG (20 μl each, in phosphate buffer, pH 7.4) were used and the mixture was analyzed (recorded for 1 min). The ESR spectrometer parameters were as follows: central magnetic field 336.8 mT, power 1.00 mW, frequency 9.4380 GHz, modulation width 0.2 mT, amplitude 600, sweep width 10 mT, sweep time 0.5 min, gain 200, time constant 0.03 s and temperature 25°C.

Single-cell gel electrophoresis

The comet assay was used to measure oxidative DNA damage (Fernando *et al.*, 2016). Cells (5×10^4 cells/well) were seeded in medium with 10 μM PG in a 1 ml microtube for 30 min and treated with UVB (30 mJ/cm^2) and/or $PM_{2.5}$ (50 μg/ml) for another 30 min. After coating with 110 μl of 0.5% low-melting agarose, the cells were immersed in a lysis buffer (2.5 M NaCl, 100 mM Na-EDTA, 10 mM Tris, 1% Trion X-100, and 10% DMSO, pH 10) for 1 h at 4°C. An electrical field (300 mA, 25 V) was used for electrophoresis. Slides were stained with

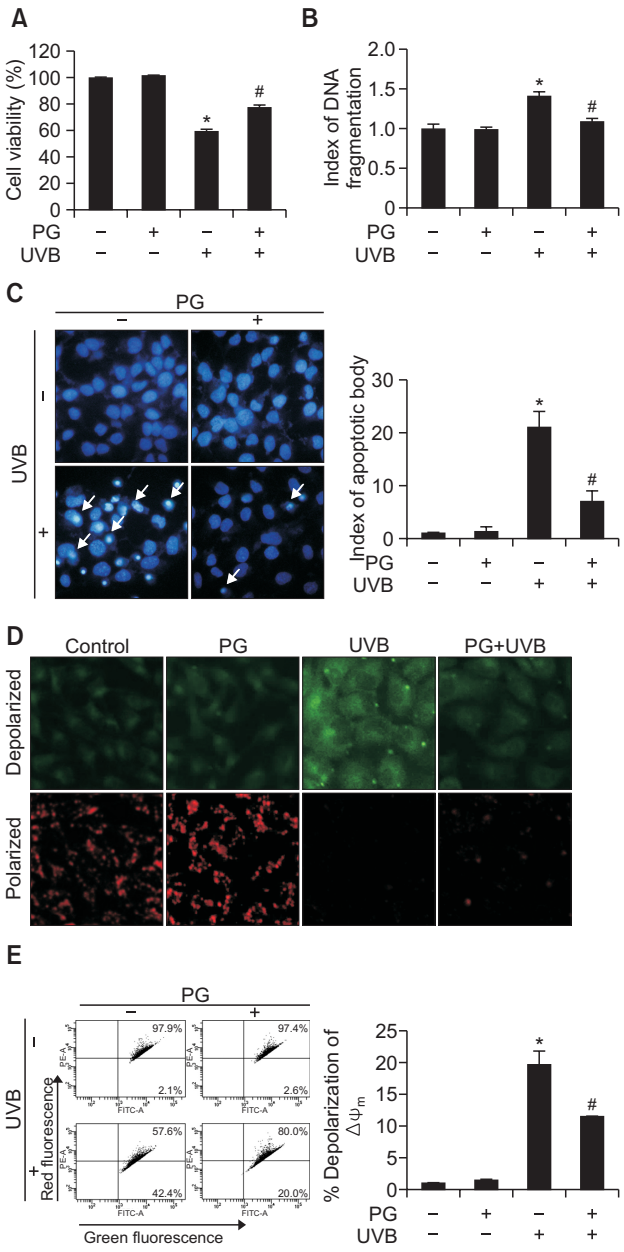

Fig. 3. PG protected cells from UVB-induced apoptosis. (A) HaCaT cell viability after UVB radiation was assessed using the MTT assay. (B) DNA fragmentation was assessed using a cellular DNA fragmentation ELISA kit. (C) Fluorescence microscopy detected apoptotic cells (arrows), stained with Hoechst 33342. The $\Delta\psi_m$ was evaluated after JC-1 staining by (D) confocal microscopy and (E) flow cytometry. *p<0.05 vs. control, $^{\#}p$<0.05 vs. UVB-irradiated cells.

50 μl of ethidium bromide (10 μg/ml) and analyzed using the Komet 5.5 image analyzer (Andor Technology, Belfast, UK). Percentage of total fluorescence and tail lengths of 50 cells per slide were recorded.

Lipid peroxidation assay

Cells were plated on a four-well chamber slide in the presence of 10 μM PG exposed to UVB (30 mJ/cm^2) and/or $PM_{2.5}$

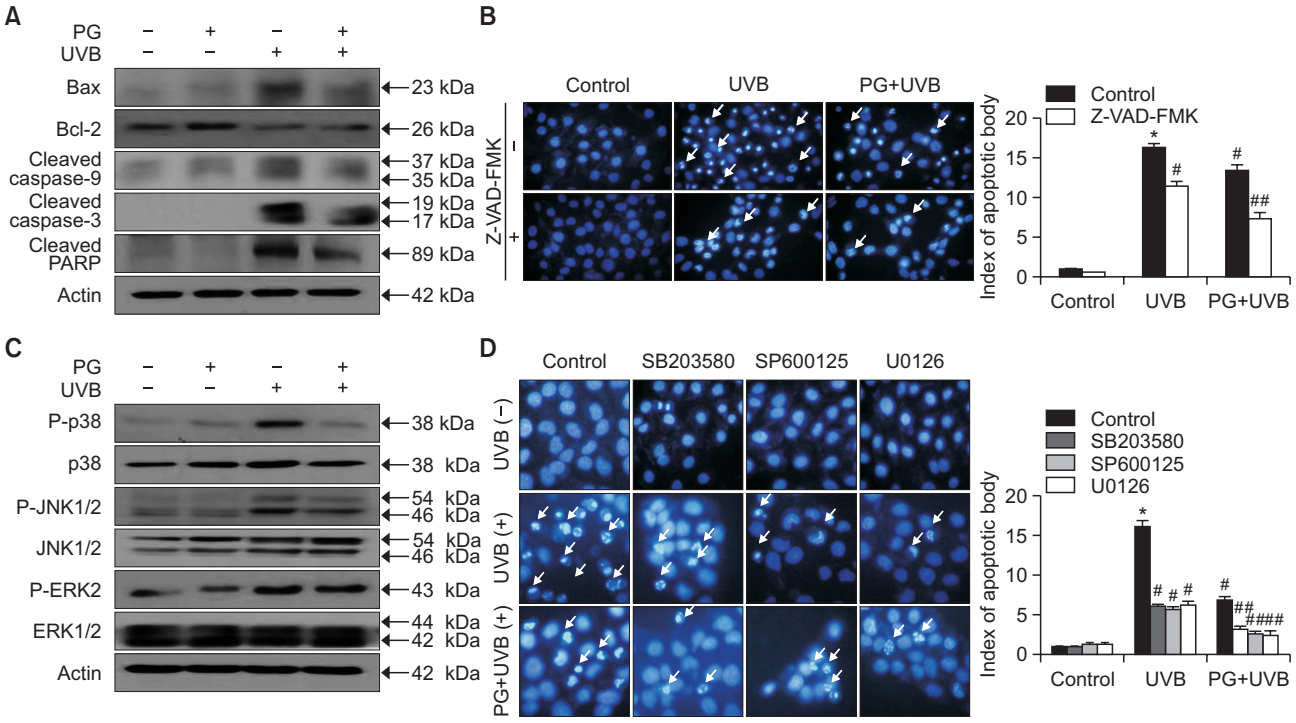

Fig. 4. PG inhibited UVB-induced apoptosis by regulation of caspase and MAPK signaling pathways. (A) Protein levels of Bax, Bcl-2, caspase-9, caspase-3, and PARP were assessed using western blotting. Actin was used as loading control. (B) Apoptotic cells pretreated with the caspase inhibitor Z-VAD-FMK and/or PG were stained with Hoechst 33342. (C) PG prevented the UVB-induced phosphorylation of p38 MAPK, JNK, and ERK, as shown by western blot. (D) Analysis of Hoechst 33342-stained apoptotic cells, after treatment with SB203580, SP600125, and U0126, which inhibit p38 MAPK, JNK and ERK, respectively. *p<0.05 vs. control, $^{\#}p$<0.05 vs. UVB-irradiated cells, $^{\#\#}p$<0.05 vs. UVB-irradiated and inhibitor-pretreated cells.

(50 μg/ml) for 5 h, and stained with DPPP for 30 min in the dark. Images were analyzed using a confocal microscope.

Detection of DNA fragmentation

DNA fragmentation was quantified using a cytoplasmic histone-associated DNA fragmentation kit (Roche Diagnostics, Mannheim, Germany).

Protein carbonylation assay

Cells were incubated with 10 μM PG for 1 h and exposed to UVB radiation (30 mJ/cm^2) or $PM_{2.5}$ (50 μg/ml) for 24 h. Protein oxidation was assessed using an Oxiselect™ Protein Carbonyl ELISA kit (Cell Biolabs, San Diego, CA, USA) according to the manufacturer's instructions.

Mitochondrial membrane potential ($\Delta\psi_m$) analysis

After treatment with 10 μM PG, the cells were exposed to UVB (30 mJ/cm^2) or $PM_{2.5}$ (50 μg/ml) for 5 h, stained with JC-1 (5 μM), and analyzed using confocal microscopy and high-performance flow cytometry.

Hoechst 33342 staining

Cells were treated with 10 μM PG for 1 h and exposed to UVB radiation (30 mJ/cm^2) and/or $PM_{2.5}$ (50 μg/ml) for 18 h. Additionally, after treatment with Z-VAD-FMK (30 μM), SB203580 (10 μM), SP600125 (10 μM), or U0126 (50 nM) for 1 h, the cells were treated with PG (10 μM) for 1 h and exposed to UVB radiation (30 mJ/cm^2) for 18 h. The cells were stained with Hoechst 33342 (20 μM) and DNA-specific fluorescence was visualized using a fluorescence microscope equipped with a Cool SNAP-Pro color digital camera. Nuclear condensation levels were evaluated and apoptotic cells were quantified.

Western blotting

Protein levels were analyzed as previously described (Cha *et al*., 2014). Membranes with proteins were sequentially incubated with the appropriate primary and secondary antibodies. Protein bands were detected by the Amersham ECL Plus Western Blotting Detection System (GE Healthcare Life Sciences, Amersham, UK).

Statistical analysis

All experiments were performed in triplicate. Data are represented as the mean ± standard error and were analyzed by the Sigma Stat (v12) software (SPSS, Chicago, IL, USA) using Tukey's test and analysis of variance (ANOVA). p-values <0.05 were considered statistically significant.

RESULTS

PG attenuates UVB-induced ROS generation

In the MTT assay, PG (Fig. 1A) did not exhibit cytotoxicity to HaCaT cells under various concentrations (Fig. 1B). Cell viability in all treated groups was >96%, similar to control. DPPH

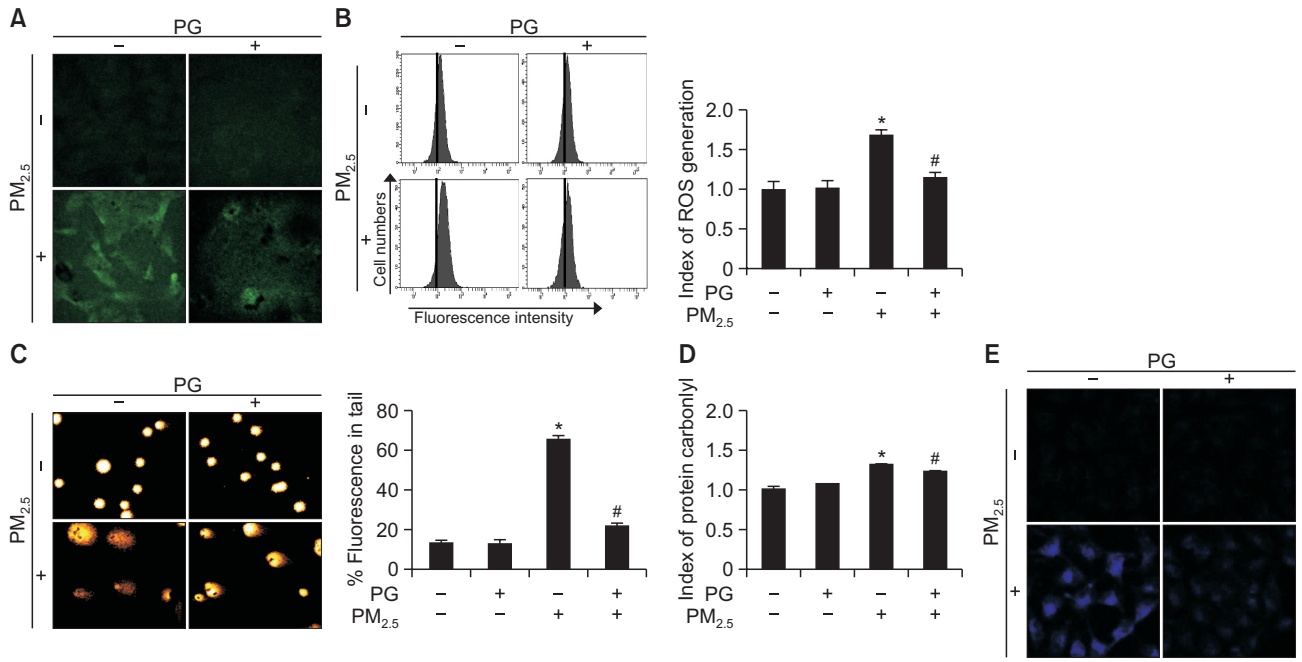

Fig. 5. $PM_{2.5}$ increased ROS generation and caused cellular damage. Intracellular ROS levels were assessed by (A) confocal microscopy and (B) flow cytometry after staining the cells with DCF-DA (green). (C) Comet assay of the DNA damage. (D) Protein carbonylation assay. (E) Lipid peroxidation was assessed after DPPP (blue) staining. *p<0.05 vs. control cells, $^{\#}p$<0.05 vs. $PM_{2.5}$-exposed cells.

radical levels were significantly decreased in a dose-dependent manner in PG-treated groups (Fig. 1C). Hydroxyl radical scavenging potential of PG (10 μM) was evaluated using ESR spectrometry. In $FeSO_4$+H_2O_2 system, DMPO/·OH adducts signal was reduced from 3366 to 2090 units by PG (Fig. 1D). In addition, DCF-DA assay indicated that H_2O_2- and UVB-induced intracellular ROS were scavenged by PG (Fig. 1E). Fluorescence spectrometry suggested that PG scavenged intracellular ROS in a concentration-dependent manner in H_2O_2- and UVB-treated cells, with 10 μM PG scavenging effect up to 42% and 19% ROS in these two cell groups respectively, compared to control. Confocal microscopy images (Fig. 1F) and flow cytometry (Fig. 1G) revealed that PG (10 μM) reduced fluorescence intensity induced by UVB radiation, indicating that PG treatment inhibits ROS generation. Taken together, these data demonstrate that PG possesses ROS-scavenging properties.

PG protects cellular macromolecules from UVB-induced damage

The protective effects of PG on UVB-induced DNA damage were evaluated by using the comet assay (Fig. 2A). The length of comet tails and percentage of tail fluorescence were significantly reduced in cells pretreated with PG compared to cells exposed to UVB (from 65 to 22%). Lipid peroxidation was analyzed using fluorescent DPPP oxide (Fig. 2B). The fluorescence intensity of DPPP oxide was higher in UVB-exposed cells, compared to that in cells treated with PG before UVB exposure. Furthermore, protein oxidation was assessed using the protein carbonylation assay (Fig. 2C). UVB irradiation significantly increased protein carbonylation, this effect ameliorated by PG pretreatment. In general, these data indicate that PG effectively blocked UVB-induced damage to macromolecules, including DNA fragmentation and oxidation of proteins and lipids.

PG suppresses UVB radiation-induced apoptosis

Cell viability after UVB irradiation was also assessed (Fig. 3A). Compared to viability of control cells (100%), cell viability was reduced upon exposure to UVB (59%), an effect ameliorated by PG pretreatment (77%). These findings suggest that PG protected cells from UVB-induced cell death. Similarly, nuclear fragmentation of PG-pretreated cells was significantly reduced, indicating that PG alleviated UVB-induced DNA fragmentation (Fig. 3B). Additionally, Hoechst 33342-stained apoptotic cells in UVB-irradiated group (Fig. 3C) displayed massive nuclear condensation; however, formation of apoptotic bodies was reduced upon PG pretreatment. JC-1 staining was used to explore apoptosis caused by disrupted mitochondrial membrane potential, with red and green fluorescence representing aggregates and monomers of the JC-1 dye, respectively. Mitochondrial depolarization resulted in intense green fluorescence in UVB-exposed cells, which was attenuated by PG treatment (Fig. 3D). Flow cytometry was used to count apoptotic bodies (Fig. 3E). UVB-irradiated cells contained the highest fraction of apoptotic cells among cell groups tested; PG pretreatment decreased the percentage of apoptotic cells from 42 to 20%. These observations suggest that PG protects cells from UVB-induced apoptosis.

PG regulates UVB-induced cell death through caspase and MAPK signaling pathways

Western blotting was used to analyze the mechanisms of PG cytoprotective effects (Fig. 4A). Levels of pro-apoptotic protein Bax were increased by UVB and decreased by PG treatment. In contrast, the levels of anti-apoptotic protein Bcl-2

were decreased by UVB and increased by PG treatment. Formation of cleaved caspase-9 and caspase-3 was stimulated by UVB exposure but reduced in PG pretreated group. Similarly, UVB irradiation induced cleavage of PARP fragments, a target of caspase-3, whereas in PG-pretreated group, levels of cleaved PARP were notably lower than levels observed in the UVB-exposed group. Apoptotic bodies in cell groups pretreated with an irreversible caspase inhibitor (Z-VAD-FMK) and/or PG decreased considerably, and PG contributing to the effects of the caspase inhibitor (Fig. 4B). To further explore signaling pathways involved in PG-mediated modulation of apoptosis, p38 MAPK, JNK, ERK and their phosphorylated forms were detected by western blot (Fig. 4C). As expected, UVB irradiation increased the levels of phosphorylated p38 MAPK, JNK, and ERK, compared to levels in cells not exposed to UVB; however, this effect was reversed by PG pretreatment. In addition, apoptotic bodies were detected by Hoechst 33342 staining (Fig. 4D). Cells pretreated with p38 MAPK, JNK, and ERK inhibitors SB203580, SP600125, and U0126, respectively, also displayed a decreased number of UVB-induced apoptotic bodies, similar to cells pretreated with PG. Furthermore, PG enhanced the anti-apoptotic effects of these inhibitors. These results demonstrate that PG activates caspase and MAPK signaling pathways and prevents UVB-induced apoptosis by regulating apoptosis-associated proteins.

PG attenuates $PM_{2.5}$-induced oxidative stress and damage to cellular macromolecules

DCF-DA assay (Fig. 5A) and cell numbers (Fig. 5B) revealed that 10 μM PG reduced the levels of $PM_{2.5}$-generated ROS. As for $PM_{2.5}$-induced DNA damage, fluorescence and length of tails were significantly reduced in the PG pretreatment group (from 65 to 22%) (Fig. 5C). Additionally, cells pretreated with PG showed lower levels of protein carbonylation than $PM_{2.5}$-exposed cells not treated with PG (Fig. 5D). $PM_{2.5}$ generated higher levels of DPPP oxide in cells not treated with PG, compared to PG-pretreated cells (Fig. 5E). These results suggested that PG suppressed $PM_{2.5}$-induced ROS generation and protected cellular macromolecules from $PM_{2.5}$-induced damage.

PG blocks $PM_{2.5}$-induced apoptosis

Using JC-1 staining, normal mitochondrial polarization was observed in $PM_{2.5}$-free cells, whereas $PM_{2.5}$-exposed cells showed indications of mitochondrial depolarization (Fig. 6A). Intensity of red and green fluorescence in PG-pretreated cells suggested higher levels of normal mitochondrial polarization and a lower degree of mitochondrial depolarization, compared to mitochondria of the $PM_{2.5}$-exposed group. Flow cytometry confirmed these observations (Fig. 6B). Additionally, Hoechst 33342 staining of apoptotic bodies indicated that $PM_{2.5}$-exposed cell group presented the highest number of apoptotic cells, whereas cells pretreated with PG avoided apoptosis to a certain degree (Fig. 6C).

PG protects cells against UVB- and $PM_{2.5}$-induced apoptosis

In order to confirm that $PM_{2.5}$ aggravates UVB-induced damage to keratinocytes, intracellular ROS levels were analyzed. Intracellular ROS levels were increased by UVB and/or $PM_{2.5}$, whereas PG (10 μM) decreased ROS levels induced by UVB and/or $PM_{2.5}$ (Fig. 7A). Lipid peroxidation was investigated by DPPP staining. $PM_{2.5}$ combined with UVB induced a high degree of lipid peroxidation, outranking UVB irradiation alone, whereas lipid peroxidation induced by UVB and/or $PM_{2.5}$ in PG-treated cells was considerably lower (Fig. 7B), indicating that PG ameliorated lipid peroxidation induced by these two factors. UVB- and/or $PM_{2.5}$-induced DNA damage was analyzed using the comet assay (Fig. 7C). Compared to UVB, $PM_{2.5}$ prolonged comet tails, whereas PG shortened comet tails in cells treated with UVB and/or $PM_{2.5}$. Additionally, Hoechst 33342 staining indicated that $PM_{2.5}$ promoted UVB-induced apoptosis, whereas pretreatment with PG partially protected the cells from UVB- and/or $PM_{2.5}$-induced apoptosis (Fig. 7D). Taken together, these results suggest that PG possesses cytoprotective effects against UVB- and/or $PM_{2.5}$-induced oxidative damage and apoptosis.

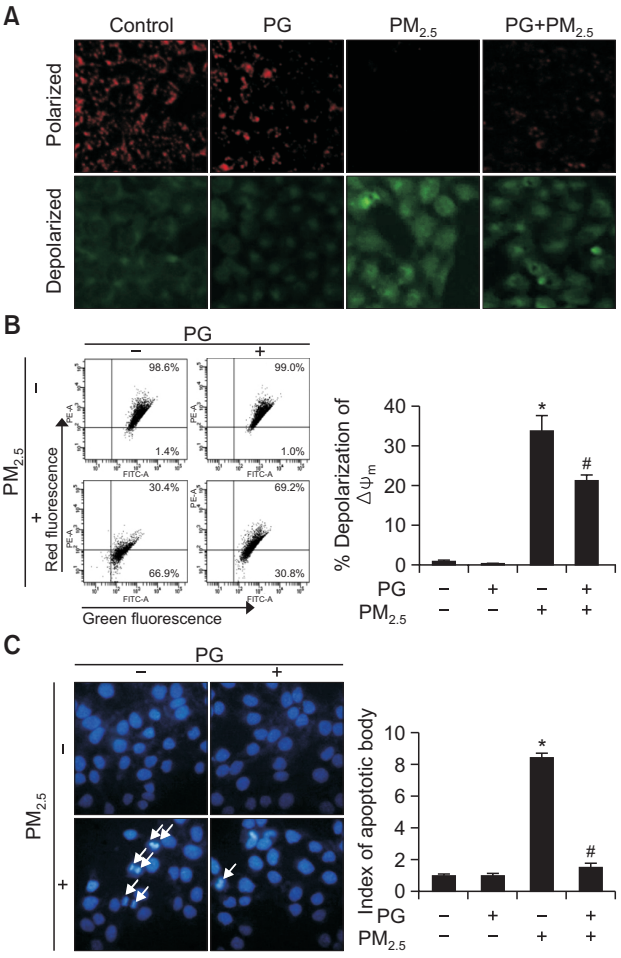

Fig. 6. $PM_{2.5}$ causes apoptosis via mitochondrial dysfunction. Cells were stained with JC-1 to detect the mitochondrial membrane potential ($\Delta\psi_m$) by (A) confocal microscopy and (B) flow cytometry. (C) Apoptotic bodies (arrows) stained with Hoechst 33342. *p<0.05 vs. control cells, #p<0.05 vs. $PM_{2.5}$-treated cells.

DISCUSSION

Skin, the largest human organ, is susceptible to irritation and sunburns through UV exposure. Moreover, epidemiologi-

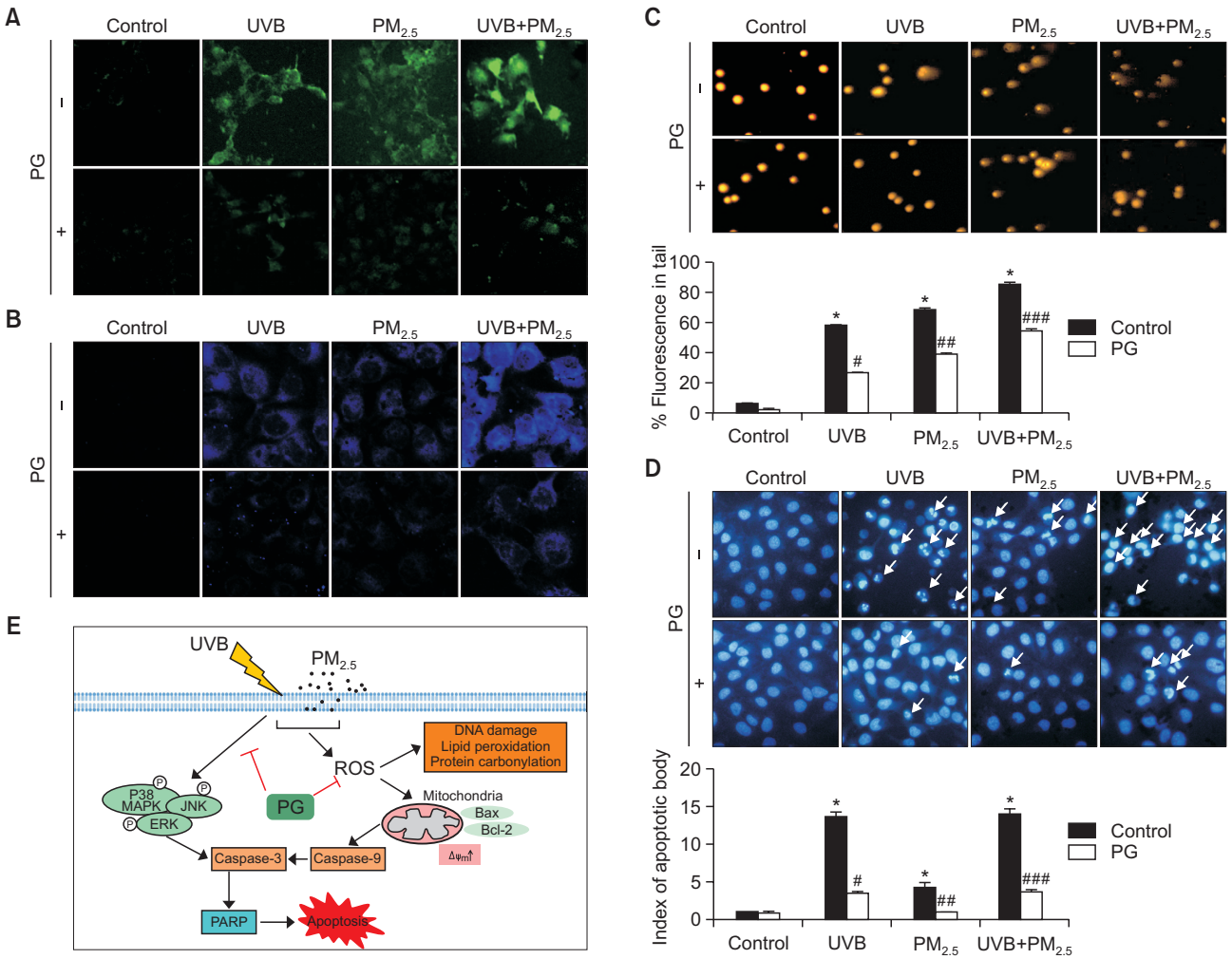

Fig. 7. $PM_{2.5}$ enhanced UVB-induced apoptosis. (A) Cells were stained by DCF-DA (green) for detecting intracellular ROS induced by UVB and/or $PM_{2.5}$. (B) Lipid peroxidation induced by UVB and/or $PM_{2.5}$ was detected after DPPP (blue) staining. (C) Comet assay cellular tail lengths induced by UVB and/or $PM_{2.5}$. (D) Fluorescence microscopy was used to detect Hoechst 33342-stained apoptotic bodies (arrows) induced by UVB and/or $PM_{2.5}$. *p<0.05 vs. control cells, $^{\#}p$<0.05 vs. UVB-irradiated cells, $^{\#\#}p$<0.05 vs. $PM_{2.5}$-treated cells, $^{\#\#\#}p$<0.05 vs. UVB-irradiated and $PM_{2.5}$-treated cells. (E) Schematic diagram of the protective mechanism of PG on UVB and $PM_{2.5}$. PG exerts cytoprotective effects by blocking oxidative-stress-induced damage to cellular components and inhibiting MAPK apoptotic signaling pathway.

cal studies have indicated that UVB suppresses immune reactions, promotes ROS generation, and damages cell membrane proteins and lipids (Boakye *et al*., 2016). UVB-induced ROS production has also been reported to be a major cause of skin cancer, as it results in the formation of 8-hydroxy-2′-deoxyguanine (Agar *et al*., 2004). Additionally, $PM_{2.5}$ (with particle diameter of <2.5 μm) can reach the lungs and stimulate ROS production in the skin, increasing oxidative stress (Piao *et al*., 2018). High ROS levels disrupt the normal function of endoplasmic reticulum, mitochondria, and lysosomes, leading to apoptosis.

This study evaluated the cytoprotective effects of PG on oxidative stress and apoptosis. Our results show that UVB and $PM_{2.5}$ increase intracellular ROS production and cause DNA fragmentation, lipid peroxidation, and protein oxidation. In human HaCaT cells, UVB and $PM_{2.5}$ exposure resulted in dysfunction of mitochondria and a high apoptosis index. Notably, $PM_{2.5}$ aggravated UVB-induced skin damage (Fig. 7), increasing oxidative stress, damaging DNA, exacerbating lipid peroxidation, and increasing the number of apoptotic bodies. PG pretreatment reduced cellular ROS levels and consequently resulted in fewer apoptotic bodies.

As predominant epidermal cells, keratinocytes protect the organism from external hazards and are inevitably influenced by complex environmental conditions. Apoptotic factors, including caspases-3 and -9 are activated under harmful conditions. Caspase-9 is a necessary factor in initiating apoptosis (Würstle *et al*., 2012). Furthermore, caspase-9 can directly activate procaspase-3 (Yin *et al*., 2006), also a key factor of apoptosis (Brentnall *et al*., 2013). In turn, caspase-3 promotes PARP cleavage (Fulda and Debatin, 2006), preventing PARP from countering DNA damage. As an example, PARP-1 is a nuclear enzyme involved in DNA fragmentation stability and regulates transcription (Rajawat *et al*., 2017). Anti-apoptotic proteins are also important participants of apoptosis. Bax/Bcl-2 proteins contribute to changes in mitochondrial perme-

ability and $\Delta\psi_m$ loss (Dlugosz *et al*., 2006), which protect cells from apoptosis induced by pro-apoptotic Bax/Bak proteins (Reed, 2006). In this study, UVB increased the protein levels of Bax, cleaved caspase-9, cleaved caspase-3, and cleaved PARP and decreased Bcl-2 levels, contributing to apoptosis. In contrast, PG treatment suppressed the increase in protein levels of Bax, cleaved caspase-9, cleaved caspase-3, and cleaved PARP, while increasing Bcl-2 levels and decreasing the number of apoptotic bodies. In order to further explore these mechanisms, we used caspase inhibitor Z-VAD-FMK, which suppressed apoptosis induced by UVB. PG contributed to anti-apoptotic effects of caspase inhibitors, which suggests that PG protects cells from apoptosis through caspase signaling pathways, by regulating the levels of apoptosis-associated proteins.

Additionally, p38 MAPK was previously shown to degrade Bcl-2 (De Chiara *et al*., 2006) and activate Bax (Kim *et al*., 2006), resulting in mitochondrial apoptotic cell death (Lee *et al*., 2008). Therefore, in the current study, we detected the expression of MAPK signaling pathway-associated proteins, including p38, JNK, and ERK. Phosphorylated p38, JNK, and ERK were up-regulated by UVB-irradiation and down-regulated by PG pretreatment. Effects of MAPK signaling pathways were further explored using p38, JNK, and ERK inhibitors. PG pretreatment inhibited phosphorylation of p38, JNK, and ERK, similar to their inhibitors and contributed to reducing the number of apoptotic bodies.

Taken together, these results show that UVB irradiation and $PM_{2.5}$ contribute to apoptosis and that PG treatment suppresses UVB-induced ROS generation, DNA damage, mitochondrial dysfunction, and protein oxidation. Furthermore, PG pretreatment inhibited UVB-induced cell apoptosis through caspase and MAPK signaling pathways by regulating key proteins participating in these pathways (Fig. 7E). These results suggest that PG could be of potential use in protecting the skin from UVB irradiation and $PM_{2.5}$.

CONFLICT OF INTEREST

The authors declare that there are no conflicts of interest.

ACKNOWLEDGMENTS

This work was supported by the Basic Research Laboratory Program (NRF-2017R1A4A1014512) using the National Research Foundation of Korea (NRF) grant funded by the Korea government (MSIP).

REFERENCES

Agar, N. S., Halliday, G. M., Barnetson, R. S., Ananthaswamy, H. N., Wheeler, M. and Jones, A. M. (2004) The basal layer in human squamous tumors harbors more UVA than UVB fingerprint mutations: a role for UVA in human skin carcinogenesis. *Proc. Natl. Acad. Sci. U.S.A.* **101**, 4954-4959.

Boakye, C. H. A., Patel, K., Doddapaneni, R., Bagde, A., Behl, G., Chowdhury, N., Safe, S. and Singh, M. (2016) Ultra-flexible nanocarriers for enhanced topical delivery of a highly lipophilic antioxidative molecule for skin cancer chemoprevention. *Colloids Surf. B Biointerfaces* **143**, 156-167.

Brentnall, M., Rodriguez-Menocal, L., De Guevara, R. L., Cepero, E. and Boise, L. H. (2013) Caspase-9, caspase-3 and caspase-7 have distinct roles during intrinsic apoptosis. *BMC Cell Biol.* **14**, 32.

Cao, J., Qin, G., Shi, R., Bai, F., Yang, G., Zhang, M. and Lv, J. (2016) Overproduction of reactive oxygen species and activation of MAPKs are involved in apoptosis induced by $PM_{2.5}$ in rat cardiac H9c2 cells. *J. Appl. Toxicol.* **36**, 609-617.

Castañeda, A. R., Pinkerton, K. E., Bein, K. J., Magaña-Méndez, A., Yang, H. T., Ashwood, P. and Vogel, C. F. A. (2018) Ambient particulate matter activates the aryl hydrocarbon receptor in dendritic cells and enhances Th17 polarization. *Toxicol. Lett.* **292**, 85-96.

Cha, J. W., Piao, M. J., Kim, K. C., Yao, C. W., Zheng, J., Kim, S. M., Hyun, C. L., Ahn, Y. S. and Hyun, J. W. (2014) The polyphenol chlorogenic acid attenuates UVB-mediated oxidative stress in human HaCaT keratinocytes. *Biomol. Ther. (Seoul)* **22**, 136-142.

Chang, C. Z., Lin, C. L., Wu, S. C. and Kwan, A. L. (2014) Purpurogallin, a natural phenol, attenuates high-mobility group box 1 in subarachnoid hemorrhage induced vasospasm in a rat model. *Int. J. Vasc. Med.* **2014**, 254270.

De Chiara, G., Marcocci, M. E., Torcia, M., Lucibello, M., Rosini, P., Bonini, P., Higashimoto, Y., Damonte, G., Armirotti, A., Amodei, S., Palamara, A. T., Russo, T., Garaci, E. and Cozzolino, F. (2006) Bcl-2 phosphorylation by p38 MAPK: identification of target sites and biologic consequences. *J. Biol. Chem.* **281**, 21353-21361.

Dlugosz, P. J., Billen, L. P., Annis, M. G., Zhu, W., Zhang, Z., Lin, J., Leber, B. and Andrews, D. W. (2006) Bcl-2 changes conformation to inhibit Bax oligomerization. *EMBO J.* **25**, 2287-2296.

Faggio, C., Sureda, A., Morabito, S., Sanches-Silva, A., Mocan, A., Nabavi, S. F. and Nabavi, S. M. (2017) Flavonoids and platelet aggregation: A brief review. *Eur. J. Pharmacol.* **807**, 91-101.

Feehan, R. P. and Shantz, L. M. (2016) Molecular signaling cascades involved in nonmelanoma skin carcinogenesis. *Biochem. J.* **473**, 2973-2994.

Fernando, P. M., Piao, M. J., Kang, K. A., Ryu, Y.S., Hewage, S. R., Chae, S. W. and Hyun, J. W. (2016) Rosmarinic acid attenuates cell damage against UVB radiation-induced oxidative stress via enhancing antioxidant effects in human HaCaT cells. *Biomol. Ther. (Seoul)* **24**, 75-84.

Fulda, S. and Debatin, K. M. (2006) Extrinsic versus intrinsic apoptosis pathways in anticancer chemotherapy. *Oncogene* **25**, 4798-4811.

Glady, A., Tanaka, M., Moniaga, C. S., Yasui, M. and Hara-Chikuma, M. (2018) Involvement of NADPH oxidase 1 in UVB-induced cell signaling and cytotoxicity in human keratinocytes. *Biochem. Biophys. Rep.* **14**, 7-15.

He, M., Ichinose, T., Yoshida, S., Shiba, F., Arashidani, K., Takano, H., Sun, G. and Shibamoto, T. (2016) Differences in allergic inflammatory responses in murine lungs: comparison of PM2.5 and coarse PM collected during the hazy events in a Chinese city. *Inhal. Toxicol.* **28**, 706-718.

Hosseini, M., Dousset, L., Mahfouf, W., Serrano-Sanchez, M., Redonnet-Vernhet, I., Mesli, S., Kasraian, Z., Obre, E., Bonneu, M., Claverol, S., Vlaski, M., Ivanovic, Z., Rachidi, W., Douki, T., Taieb, A., Bouzier-Sore, A. K., Rossignol, R. and Rezvani, H. R. (2018) Energy metabolism rewiring precedes UVB-induced primary skin tumor formation. *Cell Rep.* **23**, 3621-3634.

Kang, C. H., Rhie, S. J. and Kim, Y. C. (2018) Antioxidant and skin antiaging effects of marigold methanol extract. *Toxicol. Res.* **34**, 31-39.

Kim, B. J., Ryu, S. W. and Song, B. J. (2006) JNK- and p38 kinase-mediated phosphorylation of Bax leads to its activation and mitochondrial translocation and to apoptosis of human hepatoma HepG2 cells. *J. Biol. Chem.* **281**, 21256-21265.

Kim, K., Kim, T. H., Ihn, H. J., Kim, J. E., Choi, J. Y., Shin, H. I. and Park, E. K. (2018) Inhibitory effect of Purpurogallin on osteoclast differentiation *in vitro* through the downregulation of c-Fos and NFATc1. *Int. J. Mol. Sci.* **19**, E601.

Kong, L., Wang, S., Wu, X., Zuo, F., Qin, H. and Wu, J. (2016) Paeoniflorin attenuates ultraviolet B-induced apoptosis in human keratinocytes by inhibiting the ROS-p38-p53 pathway. *Mol. Med. Rep.* **13**, 3553-3558.

Lee, S. J., Kim, M. S., Park, J. Y., Woo, J. S. and Kim, Y. K. (2008) 15-Deoxy-delta 12,14-prostaglandin J2 induces apoptosis via JNK-mediated mitochondrial pathway in osteoblastic cells. *Toxicology*

248, 121-129.

Liu, Q., Xu, C., Ji, G. X., Liu, H., Shao, W., Zhang, C., Gu, A. and Zhao, P. (2017) Effect of exposure to ambient $PM_{2.5}$ pollution on the risk of respiratory tract diseases: a meta-analysis of cohort studies. *J. Biomed. Res.* **31**, 130-142.

Nohynek, G. J. and Schaefer, H. (2001) Benefit and risk of organic ultraviolet filters. *Regul. Toxicol. Pharmacol.* **33**, 285-299.

Oh, M. C., Piao, M. J., Fernando, P. M., Han, X., Madduma Hewage, S. R., Park, J. E., Ko, M.S., Jung, U., Kim, I. G. and Hyun, J. W. (2016) Baicalein protects human skin cells against ultraviolet B-induced oxidative stress. *Biomol. Ther. (Seoul)* **24**, 616-622.

Park, H. Y., Kim, T. H., Kim, C. G., Kim, G. Y., Kim, C. M., Kim, N. D., Kim, B. W., Hwang, H. J. and Choi, Y. H. (2013) Purpurogallin exerts anti-inflammatory effects in lipopolysaccharide-stimulated BV2 microglial cells through the inactivation of the NF-κB and MAPK signaling pathways. *Int. J. Mol. Med.* **32**, 1171-1178.

Piao, M. J., Ahn, M. J., Kang, K. A., Ryu, Y. S., Hyun, Y. J., Shilnikova, K., Zhen, A. X., Jeong, J. W., Choi, Y. H., Kang, H. K., Koh, Y. S. and Hyun, J. W. (2018) Particulate matter 2.5 damages skin cells by inducing oxidative stress, subcellular organelle dysfunction, and apoptosis. *Arch. Toxicol.* **92**, 2077-2091.

Prasad, K. and Laxdal, V. A. (1994) Evaluation of hydroxyl radical-scavenging property of purpurogallin using high pressure liquid chromatography. *Mol. Cell Biochem.* **135**, 153-158.

Rajawat, J., Shukla, N. and Mishra, D. P. (2017) Therapeutic targeting of poly(ADP-Ribose) polymerase-1 (PARP1) in cancer: current developments, therapeutic strategies, and future opportunities. *Med. Res. Rev.* **37**, 1461-1491.

Reed, J. C. (2006) Proapoptotic multidomain Bcl-2/Bax-family proteins: mechanisms, physiological roles, and therapeutic opportunities. *Cell Death Differ.* **13**, 1378-1386.

Wang, Y., Xiong, L. and Tang, M. (2017) Toxicity of inhaled particulate matter on the central nervous system: neuroinflammation, neuropsychological effects and neurodegenerative disease. *J. Appl. Toxicol.* **37**, 644-667.

Wu, T. W., Zeng, L. H., Wu, J., Fung, K. P., Weisel, R. D., Hempel, A. and Camerman, N. (1996) Molecular structure and antioxidant specificity of purpurogallin in three types of human cardiovascular cells. *Biochem. Pharmacol.* **52**, 1073-1080.

Würstle, M. L., Laussmann, M. A. and Rehm, M. (2012) The central role of initiator caspase-9 in apoptosis signal transduction and the regulation of its activation and activity on the apoptosome. *Exp. Cell Res.* **318**, 1213-1220.

Yin, Q., Park, H. H., Chung, J. Y., Lin, S. C., Lo, Y. C., da Graca, L.S., Jiang, X. and Wu, H. (2006) Caspase-9 holoenzyme is a specific and optimal procaspase-3 processing machine. *Mol. Cell* **22**, 259-268.

Zeng, L. H. and Wu, T. W. (1992) Purpurogallin is a more powerful protector of kidney cells than Trolox and allopurinol. *Biochem. Cell Biol.* **70**, 684-690.

Zheng, J., Piao, M. J., Kim, K. C., Yao, C. W., Cha, J. W., Shin, J. H., Yoo, S. J. and Hyun, J. W. (2014) Photo-protective effect of americanin B against ultraviolet B-induced damage in cultured human keratinocytes. *Environ. Toxicol. Pharmacol.* **38**, 891-900.

Zheng, W., Wang, B., Si, M., Zou, H., Song, R., Gu, J., Yuan, Y., Liu, X., Zhu, G., Bai, J., Bian, J. and Liu, Z. (2018) Zearalenone altered the cytoskeletal structure via ER stress- autophagy- oxidative stress pathway in mouse TM4 Sertoli cells. *Sci. Rep.* **8**, 3320.